Computational Model of Cytokinetic Abscission Driven by ESCRT-III Polymerization and Remodeling

Natalie Elia,[†‡△] Gur Fabrikant,[§△] Michael M. Kozlov,[§*] and Jennifer Lippincott-Schwartz[†*]
[†]Cell Biology and Metabolism Program, Eunice Kennedy Shriver National Institute of Child Health and Development, National Institutes of Health, Bethesda, Maryland; [‡]Department of Life Sciences and the National Institute for Biotechnology in the Negev, Ben Gurion University of the Negev, Beer Sheva, Israel; and [§]Department of Physiology and Pharmacology, Sackler Faculty of Medicine, Tel Aviv, Israel

ABSTRACT The endosomal sorting complex required for transport (ESCRT)-III complex, capable of polymerization and remodeling, participates in abscission of the intercellular membrane bridge connecting two daughter cells at the end of cytokinesis. Here, we integrate quantitative imaging of ESCRT-III during cytokinetic abscission with biophysical properties of ESCRT-III complexes to formulate and test a computational model for ESCRT-mediated cytokinetic abscission. We propose that cytokinetic abscission is driven by an ESCRT-III fission complex, which arises from ESCRT-III polymerization at the edge of the cytokinetic midbody structure, located at the center of the intercellular bridge. Formation of the fission complex is completed by remodeling and breakage of the ESCRT-III polymer assisted by VPS4. Subsequent spontaneous constriction of the fission complex generates bending deformation of the intercellular bridge membrane. The related membrane elastic force propels the fission complex along the intercellular bridge away from the midbody until it reaches an equilibrium position, determining the scission site. Membrane attachment to the dome-like end-cap of the fission complex drives membrane fission, completing the abscission process. We substantiate the model by theoretical analysis of the membrane elastic energy and by experimental verification of the major model assumptions.

INTRODUCTION

The physical separation of two daughter cells at the end of mitosis, known as cytokinetic abscission, involves cleavage of a narrow, microtubule-based, intercellular bridge connecting two nascent daughter cells arising during cell division (1–5). Cytokinetic abscission is thought to be coordinated at the midbody dark zone, a dense structure ~0.7 μm wide located at the center of the intercellular bridge (1–3,6). However, the very late events of bridge cleavage, culminating in abscission, do not occur at the midbody itself, but rather at a narrow constriction site ~1 μm away from the midbody center (6,7). The molecular machinery operating at this narrow constriction site to drive membrane fission has until recently been unclear. However now, advanced cell imaging and biochemical approaches implicate endosomal sorting complex required for transport (ESCRT) components in the machinery underlying final membrane abscission. That is, ESCRT proteins accumulate at the abscission site immediately before the time of abscission (6); they form spiral filaments in vitro that have similar properties to filaments seen by electron microscopy (EM) at the abscission site (7,8); and their absence leads to inhibition or delay in abscission (9–11).

The ESCRT machinery consists of five protein complexes that sequentially recruit onto membrane sites: ESCRT-0, ESCRT-I, ESCRT-II, ESCRT-III, and VPS4. Together, these complexes function as a modular machinery for driving membrane constriction and scission in many intracellular contexts, including at the multivesicular body (for intraluminal vesicle budding) and at human immunodeficiency virus (HIV) viral budding sites in the plasma membrane (12,13). Each ESCRT complex is thought to play a distinct role. The early complexes ESCRT-0, -I and -II facilitate cargo recruitment and membrane bending. The late ESCRT-III complexes comprise the core scission machinery, demonstrated by reconstitution studies in which ESCRT-III association with artificial membranes drives inward budding and fission of vesicles (14–16). VPS4, an AAA-ATPase recruited by ESCRT-III, is proposed to help disassemble and/or remodel ESCRT filaments (14,16–18). The membrane constriction and scission activity of ESCRT-III is believed to arise from its ability to form helical structures that interact with membrane (19–21). Indeed, in the presence of VPS4, ESCRT-III components polymerize in vitro into 50 nm diameter membrane tubes with dome-like end-caps (8). The external surface of these tubes has a high affinity to lipid bilayers containing acidic lipids (8). The emerging view, therefore, is that ESCRT-0-II serve as protein adaptors that recruit ESCRT-III scission activity to different membrane cellular locations. Membrane recruited ESCRT-III then assembles into a complex, which induces membrane constriction, leading to membrane fission.

In the context of cytokinesis, the details of ESCRT function in membrane remodeling and abscission remain ambiguous. Electron tomography has shown ESCRT-III-dependent filaments at the constriction site (7). These have the appropriate helical morphology of ESCRT filaments, consistent with an ESCRT-III polymer. However,

Submitted February 12, 2012, and accepted for publication April 5, 2012.

△Natalie Elia and Gur Fabrikant contributed equally to this work.

*Correspondence: lippincj@mail.nih.gov or michk@post.tau.ac.il

Editor: Edward Stuenkel.

0006-3495/12/05/2309/12 $2.00

doi: 10.1016/j.bpj.2012.04.007

analysis using superresolution microscopy revealed ESCRT-III resides at an additional site, adjacent to the midbody center as a pair of rings, during early and late stages in cytokinesis (6). The two distinct localizations of ESCRT-III during cytokinesis raise the question of whether they are interdependent and if so, what role each plays in the membrane constriction and scission events occurring during cytokinesis (6). Here, we explore these issues by suggesting and substantiating computationally and experimentally a detailed mechanism of action for ESCRT proteins in cytokinetic abscission.

We propose that ESCRT-III forms a fission complex, which drives constriction and abscission of the intercellular bridge. The ESCRT-III fission complex forms as a result of VPS4-enabled breakage of the initial ESCRT-III oligomer, polymerizing at the edge of the midbody dark zone. Once formed, the fission complex constricts to its spontaneous diameter of ~50 nm, while sliding along the intercellular bridge away from the midbody dark zone. Sliding continues until the fission complex reaches its equilibrium position corresponding to the minimal elastic energy of the bridge membrane. The subsequent abscission is driven by attachment of the bridge membrane to the dome-like end-cap of the fission complex (8,22).

Model for ESCRT-III-mediated constriction and fission of the cytokinetic tube

Relevant features of ESCRT dynamics during cytokinesis

The qualitative essence of our model is based on five sets of experimental observations related to ESCRT behavior in cytokinesis, and in vitro.

First, the ESCRT-I component TSG101 reside in a pair of large diameter (>1 μm) cortical rings located at the midbody dark zone during cytokinesis. Components of the ESCRT-III complex are recruited to the edges of the midbody dark zone, forming a pair of 1.25 μm diameter cortical ring-like structures localized symmetrically on both sides of the midbody dark zone. These partially overlap with and extend outward from the TSG101 rings (6).

Second, toward the end of cytokinesis, ESCRT-III additionally distributes asymmetrically on one side of the intercellular bridge, peripheral to the midbody dark zone (6,7). Arrival of ESCRT-III to this location is immediately followed by cytokinetic abscission, characterized by acute constriction and scission of the microtubule-based intercellular bridge (6).

Third, the ESCRT-III disassembly factor VPS4 localizes to both the midbody dark zone and the abscission site, paralleling the distribution of ESCRT-III (6). This suggests that ESCRT-III undergoes a VPS4-mediated remodeling in the area between the midbody dark zone and the abscission site.

Fourth, ESCRT-III subunits CHMP2 and CHMP3 polymerize in vitro into a helical-tubular complex of ~50 nm diameter with a hemispherical dome-like end-cap (8). The outer surface of the ESCRT-III complex has a high affinity to membrane surfaces containing acidic lipid polar heads (8).

Fifth, the ESCRT-III complexes are able to induce membrane scission in vitro when reconstituted into giant unilamellar vesicles (15).

Scenario for constriction and fission

Using the previous data, we propose the following scenario for constriction and fission of a membrane tube representing the intercellular bridge (Fig. 1). The process starts with recruitment of ESCRT-III subunits to the ESCRT-I cortical rings at the edges of the midbody dark zone. The ESCRT-I ring then serve as a template for ESCRT-III polymerization into helical complexes within the lumen of the membrane tube. The diameter of the initial turn of each of the emerging ESCRT-III helices is imposed by the dimension of the ESCRT-I rings and constitutes $D_{in} = 1.25$ μm. At the same time, the favored spontaneous diameter is determined by the intrinsic structure of the helix and is much smaller then D_{in}, constituting $D_{const} = 0.05$ μm. The mismatch between the imposed, D_{in}, and spontaneous, D_{const}, diameters results in mechanical stresses within the emerging ESCRT-III helices. These stresses promote a VPS4-mediated breakage of the ESCRT-III polymer into two parts. The first part consisting of the initial ESCRT-III ring remains attached to the ESCRT-I cortical ring, whereas the second, representing the fission complex, is free to relax to its spontaneous diameter. The generated fission complex completes its polymerization into a narrow cylinder of 0.05 μm diameter with a dome-like end-cap.

Both the initial ESCRT-III ring and the emerging fission complex stick to the inner side of the membrane tube due to electrostatic interactions. Although the former is immobilized by its connection to the ESCRT-I ring, the latter can slide along the tube due to the lateral mobility of lipid molecules mediating the protein-membrane interaction. This mobility may be restricted by lipid domain formation, which can serve as a regulator of the fission reaction.

The portion of the membrane tube attached to the initial ESCRT-III ring is constrained to have the cross-section diameter of $D_{in} = 1.25$ μm, whereas the membrane portion attached to the scission complex gets constricted down to the small diameter of $D_{const} = 0.05$ μm. This results in a strong deformation of the membrane tube between the two ESCRT-III structures, with accumulation of corresponding elastic energy (23). The calculations below demonstrate that this energy depends on the distance between the initial ESCRT-III ring and the fission complex and has a minimum at a certain distance corresponding to the equilibrium position of the scission complex. Hence, relaxation of the scission complex to its spontaneous diameter results in its sliding away from the midbody dark zone, mediated by the elastic energy of the intercellular bridge membrane until it reaches its equilibrium position.

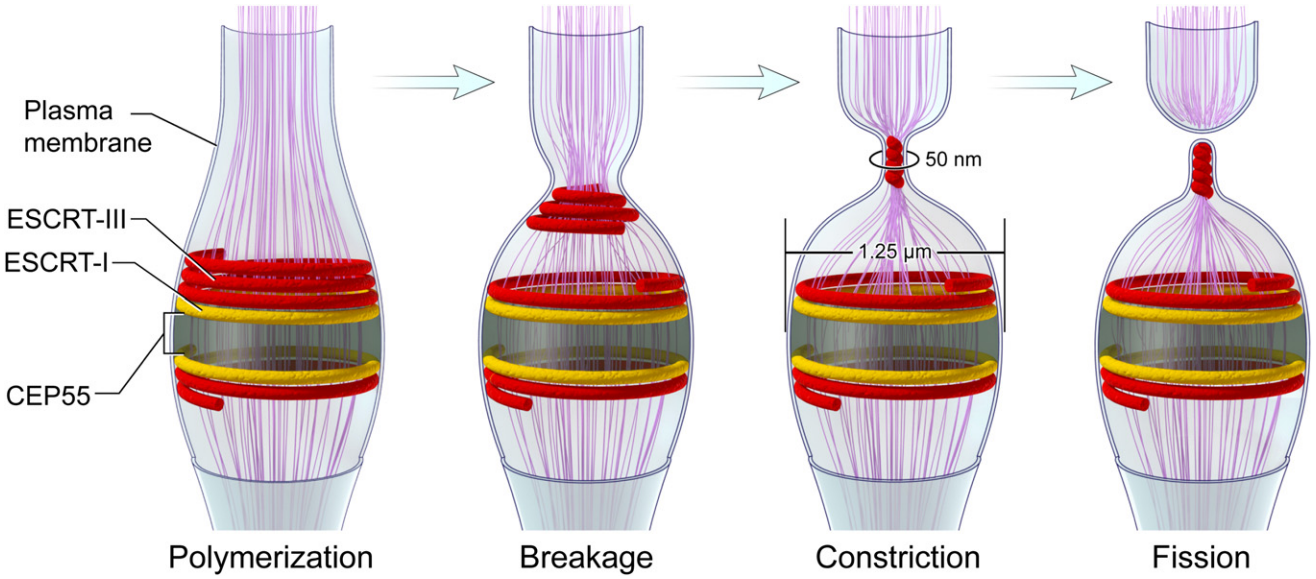

FIGURE 1 Mechanistic model for ESCRT-III-mediated abscission. Late in cytokinesis, the ESCRT-III complex (*red*) is recruited to the center of the intercellular bridge by early ESCRT components and assembles in two initial rings on both sides of the midbody dark zone. Close to abscission, the ESCRT-III complex begins polymerizing into a spiral on one side of the microtubule bridge. This polymerization is followed by a VPS4-mediated rearrangement of the spiral into two distinct pools. An initial pool that retains a large diameter of ~1.25 μm, imposed by the early ESCRT protein TSG101 (*yellow*), and a fission complex that is free to constrict to its preferred diameter of 0.05 μm. The fission complex slides along the intercellular bridge and constricts until it reaches its equilibrium distance, which is determined by elastic forces in the membrane that resist such constriction. As a result, the membrane of the intercellular bridge, which is attached to the ESCRT-III complex via electrostatic interaction, gets constricted. Once the fission complex reaches its equilibrium position, ESCRT-III-mediated fission of the intercellular bridge occurs via membrane attachment to the dome-like end-cap of the ESCRT-III fission complex leading to complete separation of the two daughter cells. Microtubules are depicted in purple. Arrows represents the transition from early to late time points during the abscission process.

The subsequent attachment of the bridge membrane to the dome-like end-cap of the scission complex drives membrane fission according to the mechanism analyzed in Fabrikant et al. (22). Abscission on the other side of the intercellular bridge occurs by a similar mechanism.

MATERIALS AND METHODS

Cell culture and transfection

Madin-Darby canine kidney (MDCK) II cells were grown in Eagle's minimal essential medium supplemented with 10% fetal bovine serum, 2 mM glutamine, 100 IU/ml penicillin, and 100 mg/ml streptomycin. Transfection with the plasmids listed below was carried out using Lipofectamine 2000 (Invitrogen) according to the manufacturer guideline. Live cell imaging was performed 16–40 h posttransfection. When CHMP4B-mcherry was transfected low expressing cells that showed a uniform cytosolic localization of CHMP4B-mCherry were imaged live or fixed.

Plasmid constructs

Full-length human CHMP4B-Flag, CHMP2A-Flag, and CHMP5-Flag were kindly provided by Dr. Wesley Sundquist (University of Utah, School of Medicine, UT).

CHMP4B-mCherry

Full-length human CHMP4B was cloned to mCherry-C1 vector as previously described and characterized (6).

Tubulin-GFP

Full-length human α-tubulin was cloned into pEGFP-C1 as previously described (6).

All plasmids were sequenced.

Mitotic synchronization

Where indicated, cells were subjected to aphidicolin treatment (2.5 g for 16 h) 16 h posttransfection. Cells were then released from the aphidicolin treatment and fixed 11–12 h later for 10 min with 4% PFA. These incubation times maximized the percentage of cells undergoing cytokinetic abscission.

Fixation and immunostaining

Cells were fixed with 4% PFA for 10 min, blocked with 10% fetal bovine serum and stained with monoclonal α-tubulin antibodies (DM1A, Sigma) and with Rabbit polyclonal Flag antibodies (kindly provided by Dr. Ramanujan Hedge, NIH, MD). Cells were then subjected to a secondary antibody staining with the suitable Alexa-488 or Alexa-546 antimouse or antirabbit secondary antibodies (Invitrogen). Finally, cells were mounted with Fluoromount-G (SouthernBiotech, Birmingham, AL).

Metabolic ATP depletion

MDCK cells expressing CHMP4B-mCherry and tubulin-GFP were incubated in Dulbecco's modified Eagle's medium no glucose media containing 25 mM deoxyglucose and 10 mM Na_3N for 20 min before imaging. Control experiments in MDCK cells expressing tubulin-GFP alone showed similar

phenotypes indicating that the phenotype observed are not an artifact of the CHMP4B-mCherry overexpression.

Image acquisition

Z stacks of MDCK cells expressing the designated proteins were collected using a confocal spinning disk microscope (Marianas; Intelligent Imaging, Denver, CO) and video recorded on an EM-CCD camera (evolve, Photometrics, Tucson, AZ). A 63X oil objective was used for imaging fixed cells (pixel size = 0.11 μm) and a 40X oil objective was used for live cell imaging (pixel size = 0.174 μm). Image processing and image analysis were done on maximal projection images using Slidebook 5 (Intelligent Imaging). To reduce background noise images were subjected to a nearest neighbor deconvolution algorithm. For imaging of CHMP4B-mCherry only cells that showed a uniform dim cytosolic distribution were imaged and analyzed. These cells were previously shown to undergo normal cytokinesis (6). Microtubule diameter was determined based on the microtubule fluorescence intensity profile of a line positioned at the most constricted region ~1 μm away from the center of the midbody (from both sides) perpendicular to the intracellular bridge. The distance between the two CHMP4B-Flag pools was determined as the distance between the end of the initial pool and the beginning of the second pool from the intensity profile of a line positioned along the intercellular bridge. Similar methodology was applied to measure the distance between the end of the dark zone and the constriction/scission site based on microtubule fluorescence (see Fig. 6 *a*). The relative spread of CHMP4B-mCherry (see Fig. 4 *b*) was determined from a line intensity profile positioned along one side of the intercellular bridge. In those experiments the line intensity profile on each side of the intercellular bridge was continuous and did not show the characteristic two distinct pools shown in Fig. 2, *b–d*.

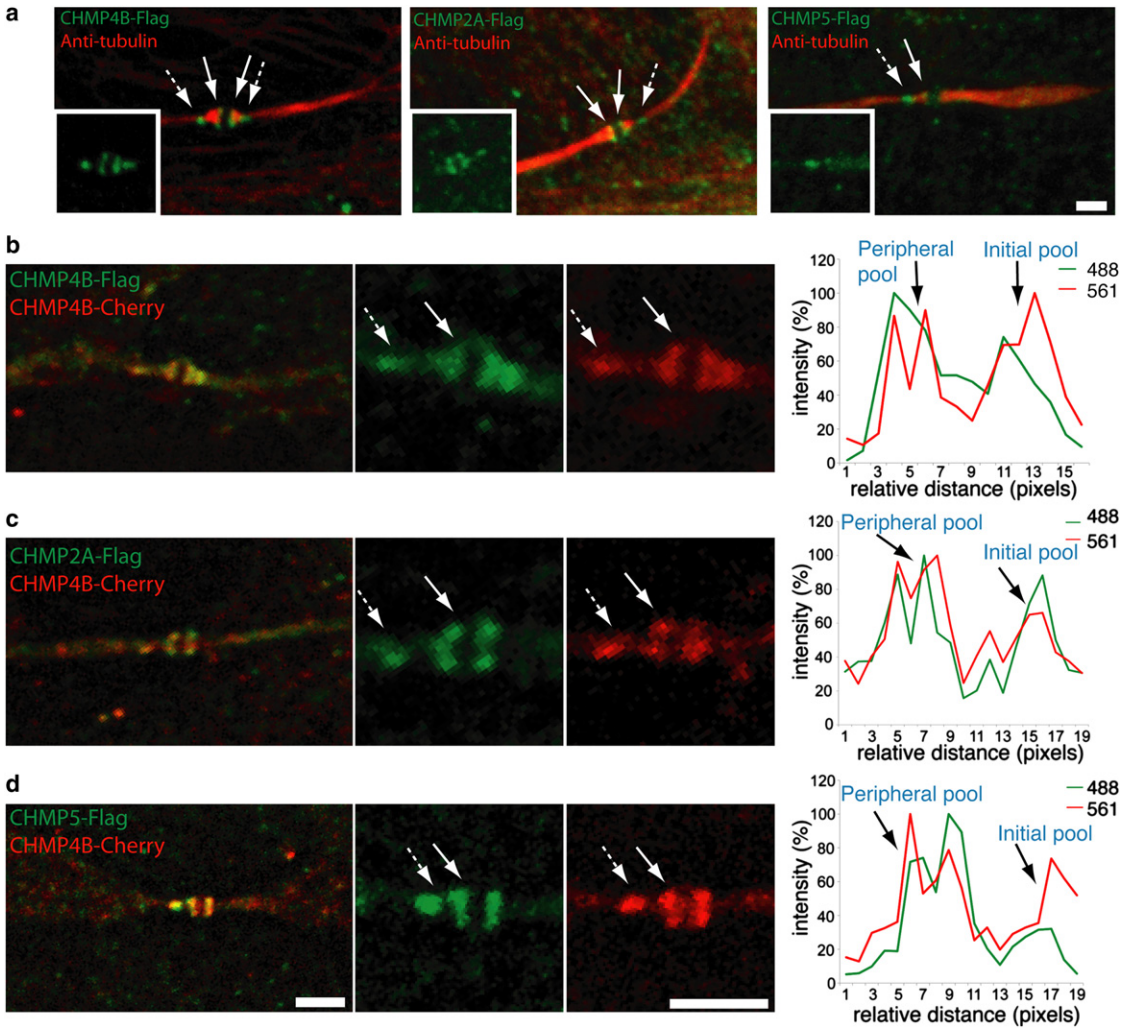

FIGURE 2 ESCRT-III resides in two spatially distinct pools in intercellular bridges undergoing abscission. (*a*) Synchronized MDCK cells expressing Flag-tagged versions of CHMP4B, CHMP2A, or CHMP5 (from *left* to *right*) were fixed, stained with anti-α-tubulin (*red*) and anti-Flag (*green*) antibodies and imaged using a spinning disk confocal microscope. CHMP4B, CHMP2A, and CHMP5 localized in two spatially distinct pools; an initial pool located to the edge of the midbody dark zone (*solid arrows*) and a peripheral pool located at the site of microtubule constriction (*dashed arrows*). (*b–d*) Synchronized MDCK cells expressing CHMP4B-mCherry (*red*) together with either CHMP4B-Flag (*b*), CHMP2A-Flag (*c*), or CHMP5-Flag (*d*) were stained with anti-Flag antibodies (*green*) and imaged. Anti-α-tubulin staining was used to identify the intercellular bridges (not shown). Data show a high degree of overlap between the localization of CHMP4B-mCherry and either CHMP2A or CHMP5 on both the initial pool (*solid arrows*) and the peripheral pool (*dashed arrows*). Right panels show intensity profiles of a line drawn along the intercellular bridge between the ESCRT-III peripheral and initial pools. Similar data were obtained for all the ESCRT-III components examined. Scale bar = 2 μm. *n* (for each panel) = 10. Similar localization pattern and overlap between the pools were observed in all cells examined. Data were obtained from two independent experiments.

RESULTS

ESCRT-III is organized into two, spatially separated complexes between the midbody dark zone and abscission site

To substantiate the previous model, we began by testing whether late in cytokinesis ESCRT-III components are organized into two separate complexes. These two complexes would include the ESCRT-III ring at the edge of the midbody dark zone and the fission complex. We have previously reported that the ESCRT-III component CHMP4B localizes in two spatiotemporally distinct pools; one at the midbody center and another at the abscission site (6). However, ESCRT-III is a heterogeneous protein complex composed of several CHMP proteins. Recruitment of CHMP4B into the complex is followed by recruitment of the CHMP2 and CHMP3 complexes and by ESCRT-III-like members such as CHMP5 (14,21). The two seemingly separate ESCRT-III complexes seen at the midbody dark zone and at the abscission site (6), therefore, could represent a single, polarized ESCRT-III structure interconnected by nonlabeled ESCRT-III proteins. To rule out the existence of a continuous ESCRT-III structure at the end of cytokinesis, we examined the localization of FLAG-tagged versions of CHMP4B, CHMP2A, and CHMP5 in the intercellular bridge of cells undergoing abscission. Notably, CHMP4B, CHMP2A, and CHMP5 were all localized in two distinct pools on one side of the intercellular bridge, with the more peripheral pool of each localizing at the site of microtubule constriction (Fig. 2 *a*). Synchronized MDCK cells coexpressing both CHMP4B-mCherry and FLAG-tagged versions of either CHMP2A or CHMP5 close to the time of abscission revealed these proteins always had a high degree of colocalization, both at the peripheral site and at the edge of the midbody dark zone (Fig. 2, *b–d*).

Given different ESCRT-III components show the same overall pattern of distribution, and also exhibit a distinct and similar gap between central and peripheral pools (Fig. 2, *b–d*, see intensity graphs), we concluded that ESCRT-III components do not extend as a continuous filament from the edge of the midbody dark zone to the peripheral, constriction site. Rather, ESCRT-III proteins localize in two spatially distinct structural pools: one found centrally, rimming the midbody dark zone and the other found peripherally, at the constriction site, supporting our model assumption.

ESCRT-III fission complex originates at the location of the initial ESCRT-III complex, moves outward, and stabilizes at a conserved distance from its point of origin

A key aspect of the proposed model is that the two separate ESCRT-III complexes found at the central midbody region and at the peripheral constriction site are spatiotemporally related. To test this, we analyzed the relationship between the two ESCRT-III complexes at different times during cytokinetic abscission. CHMP4B was used for this analysis because it is the most abundant protein of the ESCRT-III complex and one of the earliest to assemble (14,21). Early through late stages of the abscission process were distinguished based on the microtubule diameter found in the cytokinetic bridge, which dramatically decreases as abscission progresses (6,7). During early stages of the abscission process, we found that CHMP4B localized only to the central ESCRT-III pool adjacent to the midbody center (Fig. 3 *a*). CHMP4B often extended peripherally off one of the sides toward the direction of the constriction zone (see *arrow*). At mid-to-late stages, a second population of CHMP4B appeared, locating peripherally to one side of the intercellular bridge. At postabscission stages, represented by a midbody remnant, CHMP4B was observed at both the abscission sites as well as in the central pools.

Measurement of the distance between the two ESCRT-III pools in the cytokinetic intercellular bridge as a function of microtubule diameter revealed the peripheral ESCRT-III pool distributes further away from the central ESCRT-III pool as abscission progresses (assessed by microtubule diameter change) (Fig. 3 *b*). This continued until a conserved distance of ~0.7 μm was reached between the central and peripheral pools (Fig. 3 *b*). From this point on, further tightening of the microtubule bundle was no longer accompanied by an increased distance between the pools. Notably, ~0.7 μm was also the characteristic distance measured between the central and peripheral CHMP4B pools in midbody remnants, implying that it represents the gap between the two ESCRT-III pools at the time of abscission. Together, the data suggested that the second ESCRT-III pool moves progressively away from the initial midbody-localized pool until it reaches a conserved distance from the initial pool (Fig. 3 *c*). At this distance, membrane constriction and abscission occurs.

The previous data support the view that the ESCRT-III fission complex originates at or very near the initial ESCRT-III complex, but whether this occurs by splitting from the initial ESCRT-III complex, or, alternatively, by nucleation in close proximity to the initial ESCRT-III complex cannot be distinguished by our imaging approach. The first scenario is favored, however, by the results below, which examine the AAA-ATPase VPS4, a recognized disintegrator of ESCRT-III polymers.

Formation of the two ESCRT-III complexes is ATP-dependent supporting a role for VPS4

To evaluate the suggested role for VPS4 in the model, we acutely inhibited VPS4 in cells undergoing cytokinetic abscission by ATP depletion, avoiding chronic inhibition of VPS4 using siRNA depletion or a dominant negative mutant because of the previously described roles of VPS4 in early mitosis (11). When cells expressing CHMP4B-mCherry and tubulin-GFP were subjected to acute metabolic

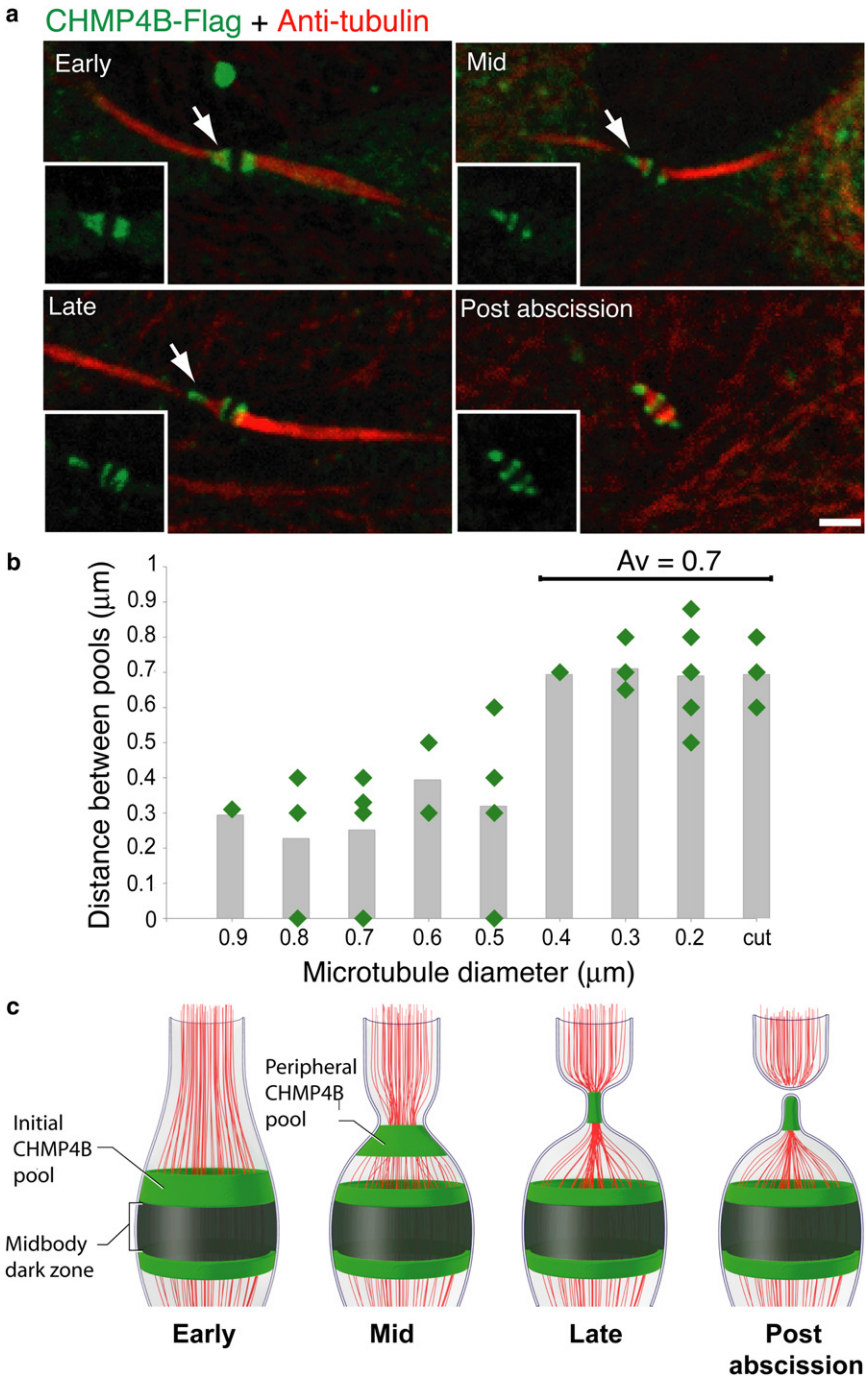

FIGURE 3 ESCRT-III fission complex originates at the location of the initial ESCRT-III ring and migrates to a conserved distance. Synchronized MDCK cells expressing CHMP4B-Flag were stained with anti-α-tubulin (*red*) and anti-Flag (*green*) antibodies. (*a*) Images show typical localization patterns observed for CHMP4B at intercellular bridges of cells undergoing abscission. The time course of abscission (early – postabscission) was determined based on the microtubule diameter measured on the side of the intercellular bridge that is undergoing constriction (see *arrow*). (*b*) Distribution of the distances measured between the initial and peripheral CHMP4B pools as a function of microtubule diameter. The distance between the CHMP4B pools was measured on either side of the intercellular bridge, when applicable, and correlated to the minimum value of microtubule diameter measured on that side. When a continuous elongated initial pool of CHMP4B was observed (as in *a* early) the distance between the pools was given a 0 value. Distances smaller than 0.2 μm were not measured due to the resolution limit of confocal microscopy and were given a 0 value. Average values for each microtubule diameter are shown as columns. Notably, the distance between the two ESCRT-III pools stabilizes in intercellular bridges with a diameter of 0.4 μm or smaller. The average distance determined for these diameters was 0.7 $\pm$ 0.1 μm. $n = 26$. (*c*) Schematic representation for ESCRT-III distribution (green) at the intercellular bridge during cytokinetic abscission. Microtubules are labeled in red.

ATP depletion in late cytokinesis, CHMP4B signal extended peripherally from the midbody dark zone. Overtime, CHMP4B formed one elongated structure in the area between the midbody center and the constriction zone (Fig. 4, *a* and *b*). No appearance of the characteristic two ESCRT-III pools occurred over 3 h of imaging (compare intensity graphs in Fig. 2, *b–d*, with intensity graph in Fig. 4 *b*). Extension of the ESCRT-III structure toward the constriction zone involved narrowing of the intercellular bridge (Fig. 4 *c*), implying the two events are linked. However, no abscission of the intercellular bridge occurred even after 9 h (Fig. 4 *d*). Similar results were obtained with overexpression of either CHMP2A-mCherry or CHMP5-mCherry (not shown). Under ATP depletion, therefore, the central midbody complex of ESCRT-III becomes continuous with the peripheral complex and no abscission occurs.

The previous observations support the model suggestion that the peripheral ESCRT-III complex arises from the initial one through an ATP-dependent remodeling mechanism. As an AAA-ATPase, VPS4 mediates the disassembly of the

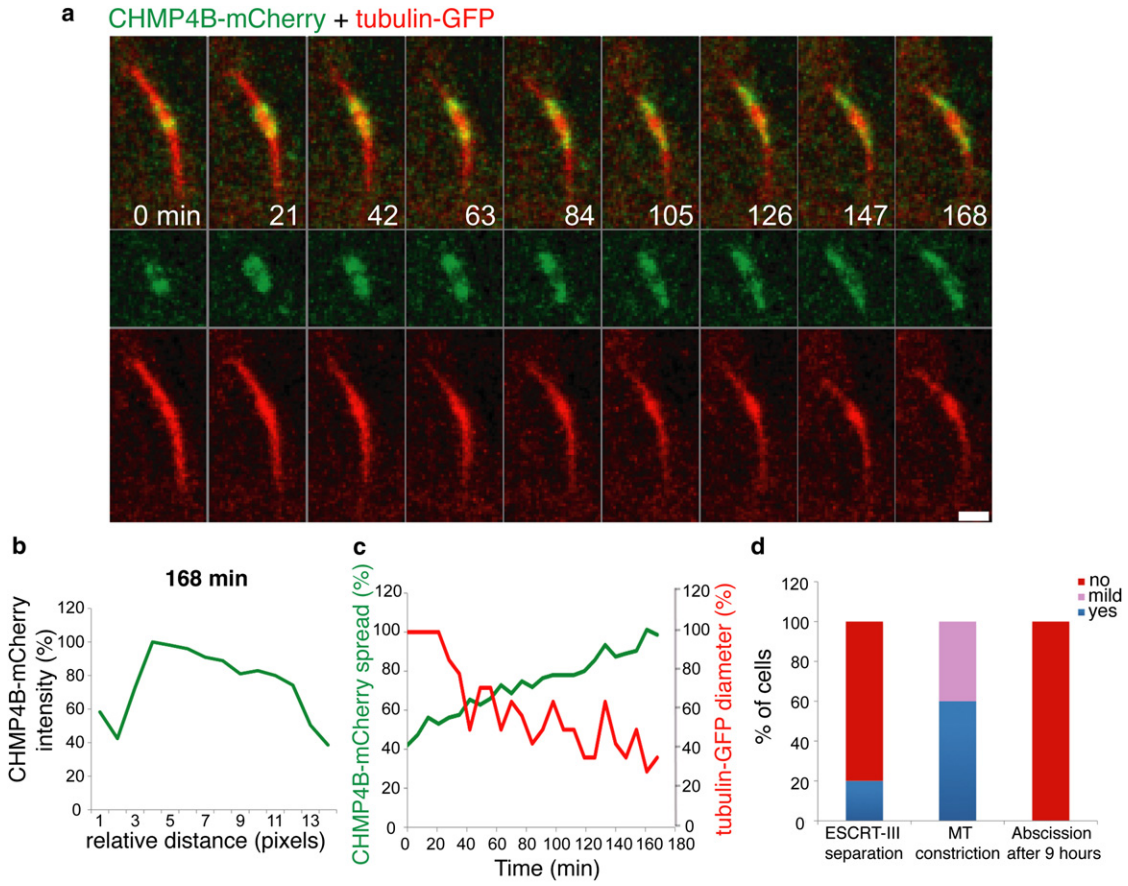

FIGURE 4 Separation of the central ESCRT-III complex into two distinct complexes is ATP dependent. Live MDCK cells expressing CHMP4B-mCherry (*green*) and tubulin-GFP (*red*) were subjected to acute ATP depletion (as described in Materials and Methods) and imaged during cytokinesis at 7 min intervals. (*a*) Representative images of every third frame from the movie sequence are shown. The overlay image is shown in the upper panel and the individual channels are shown below. (*b*) Line intensity profile of CHMP4B-mCherry on one side of the intercellular bridge at $t = 168$ min showing the continuity of the signal along the intercellular bridge and the lack of the characteristic two distinct ESCRT-III pools described in Fig. 2, *b–d*. (*c*) Measurements of the relative spread of CHMP4B-mCherry signal along one side of the intercellular bridge (*green*) and the relative microtubule diameter measured on this side (*red*) (see Materials and Methods). Shown is a representative example of 10 independent experiments. A summary of all the experiments conducted and the parameters evaluated is shown in *d*. Scale bar = 2 μm.

ESCRT-III complex (17), and is the only other component of the ESCRT machinery that has been shown to localize both to the edge of the midbody dark zone and the abscission site (6). The observed ATP dependence is thus consistent with an active role for VPS4 in mediating the separation of the two ESCRT-III complexes. It should be noted, however, that these results might additionally reflect a role for the AAA-ATPase microtubule severing enzyme spastin in the separation of the ESCRT-III complexes. However, this possibility is somewhat less likely as ESCRT-III dependent cortical filaments at the constriction site appeared to be normal in spastin-depleted cells (7).

Computation of the equilibrium distance between the midbody dark zone and the constriction-abscission site

We next sought to compute the equilibrium position of the fission complex with respect to the initial ESCRT-III ring. We consider a fragment of the intercellular bridge represented by a membrane tube of varying cross section spanned between the initial ESCRT-III ring of diameter $D_{in} = 1.25$ μm located at the edge of the midbody dark zone, and the fission complex of diameter $D_{const} = 0.05$ μm (Fig. 5 *a*). Both ESCRT-III complexes are attached to the internal side of the tube due to electrostatic interactions with the lipid polar heads. The distance between the two protein complexes and, hence, the length of the tube is denoted by L. The tube membrane is inhomogeneously bent and, therefore, is characterized by the bending elastic energy, F_B, whose value depends on L. The area of the tube membrane is taken to be variable because the membrane is supposed to be able to slip with respect to the fission complex and, hence, the tube is able to freely exchange the lipid material with the bulk of the intercellular bridge membrane serving as a lipid reservoir. The lateral tension of the membrane reservoir is assumed to vanish so that the bending energy is the only contribution to the free energy

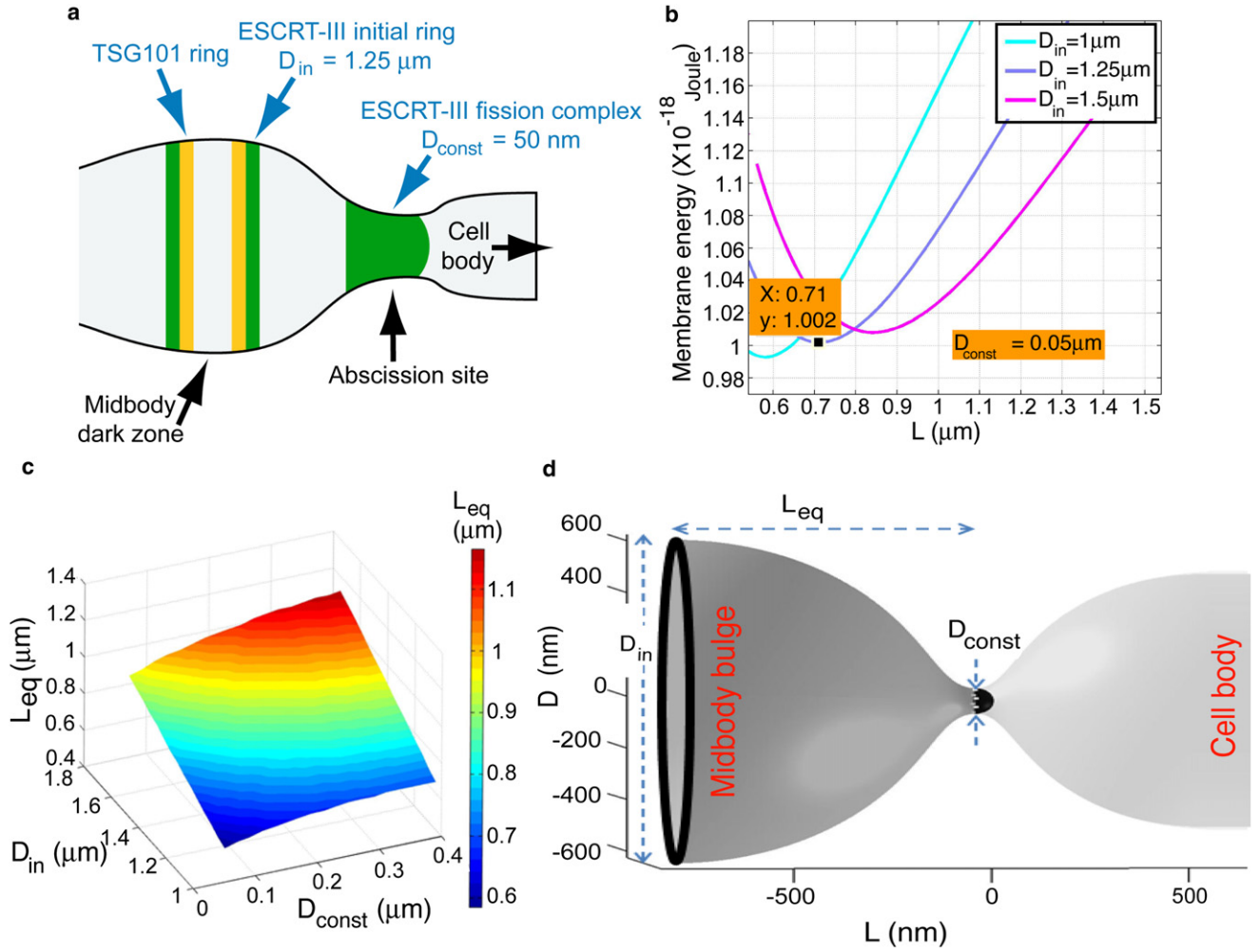

FIGURE 5 Computational analysis of the equilibrium distance between the two ESCRT-III complexes. (*a*) Schematic representation of the localization of ESCRT components in intercellular bridges of cells considered in our model. The initial diameter of ESCRT-III (D_{in}) is based on our previous direct measurements of the diameter of CHMP4B rings located at the edge of the midbody dark zone (6). The diameter of the ESCRT-III peripheral pool in the abscission site (D_{const}) is taken as the spontaneous diameter measured for the ESCRT-III complex in vitro (8). ESCRT-I is depicted in yellow. ESCRT-III is depicted in green. (*b*) The bending elastic energy of the membrane between the two ESCRT-III pools as a function of the distance between the ESCRT-III pools. The three curves correspond to different diameters of the initial pool. $D_{in} = 1$ (*light blue*), 1.25 (*purple*), 1.5 μm (*magenta*), whereas the diameter of the narrow constriction pool is taken $D_{const} = 0.05$ μm. The curves show the energy minimum corresponding to the equilibrium distance L_{eq}. (*c*) The equilibrium distance, L_{eq}, as a function of the diameter of the initial pool, D_{in}, and the diameter of the peripheral pool, D_{const}. (*d*) A representative computed shape of the lipid membrane between the two ESCRT-III pools: the initial pool at the edge of the midbody dark zone and the peripheral pool at the constriction site. The computed distance between the pools corresponded to $D_{in} = 1.25$ μm and was $L_{eq} = 0.71$ μm (see graph in *b*). The constriction diameter in this frame is taken to be $D_{const} = 0.1$ μm for better visualization.

of the membrane tube. Our goal is to compute the equilibrium distance between the initial ESCRT-III ring and the fission complex corresponding to the minimal bending energy of the membrane tube and to determine the tube equilibrium shape.

The contribution to the bending energy per unit area of the membrane, f_B, relevant for the present calculation is given by the Helfrich formula, $f_B = \kappa_B J^2/2$, where κ_B is the membrane bending modulus and J is the total curvature of the membrane surface (23). The total bending energy F_B is given by integration of f_B over the area of the membrane tube.

Our analysis consists of two steps. First, for every given distance L, we find the optimal shape of the tube and the corresponding bending energy $F_B(L)$ by computing the energy of different axially symmetrical membrane shapes and finding the shape of minimal energy. The boundary conditions for this calculation are that the vector tangential to the membrane profile is parallel to the tube axis at the points where the membrane is attached to the ESCRT-III initial ring and the fission complex. The computations and the optimal shape determination have been performed numerically using the Comsol Multiphysics software.

Second, we repeat this computation for a range of distances. The results of the latter computation (presented in Fig. 5 *b*) show that the energy possesses a minimal value $F_B(L_{eq})$ for a certain distance L_{eq} serving as the equilibrium distance. We computed the L_{eq} values for some ranges of the diameters of the initial ESCRT-III rings, D_{in}, and the fission complex D_{const} as presented in Fig. 5 *c*. The computed equilibrium distance for the characteristic values $D_{in} = 1.25$ μm (6) and $D_{const} = 0.05$ μm is $L_{eq} = 0.71$ μm and the corresponding computed shape of the membrane is presented on Fig. 5 *d*. The calculated equilibrium distance and the computed shape fits very well with the overall morphology observed for cytokinetic abscission and with the conserved distance we have measured between the two CHMP4B pools in cells undergoing abscission (see Fig. 3), strongly supporting our model.

Experimental verification of the equilibrium distance

Our model predicts that the equilibrium distance between the two ESCRT-III structures ultimately dictates the site of abscission. This means that abscission should occur at a conserved distance from the edge of the midbody dark zone, where the initial ESCRT-III structure assembles. To test this experimentally, we measured the distance between the edge of the midbody dark zone, characterized by lack of microtubule staining, and the narrow constriction site in synchronized untransfected MDCK cells stained with α-tubulin antibodies. To ensure that our measurements were performed on those narrow constriction sites committed to cleavage, we only selected for measurement intercellular bridges that either exhibited asymmetric constriction or were cut on at least one side of the bridge, as shown in Fig. 6 *a*. The results revealed a clear preference to distances of ~0.6–0.8 μm, with an average distance of 0.76 ± 0.15 μm ($n = 157$) (Fig. 6 *a histogram*). Taking into account that, due to the length of the fission complex, this distance is expected to be slightly larger than the net distance between the two ESCRT-III structures and the error of our measurements (pixel size = 0.11 μm), these measurements are in good agreement with the equilibrium distances predicted by our model (Fig. 5, *b* and *c*). Moreover, in intercellular bridges with two cleavage sites (see Fig. 6 *a*, *third* and *forth panels*) we observed practically the same distance between the midbody dark zone and the narrow constriction site on either side of the midbody dark zone (average distance of 0.75 ± 0.16 μm $n = 59$ versus average distance of 0.77 ± 0.16 μm, $n = 59$). This suggests that the same physical principles apply for both sides of the midbody dark zone, as expected from our model. The consistency of the experimentally measured values with our computed values for the equilibrium distance supports our predictions for the mechanical forces that control cytokinetic abscission.

Computational analysis of fission of the constricted membrane tube mediated by membrane attachment to the dome-like end-cap of the ESCRT-III fission complex

To finalize the abscission process, constriction of the intercellular bridge should be followed by a scission event. We therefore analyzed theoretically whether the membrane fission event per se can be driven by ESCRT-III. Previously, we substantiated by a computational model that ESCRT-III-mediated fission could be induced by membrane attachment to the ESCRT-III dome structure located at the tip of the ESCRT-III helical polymer (8,22). Wrapping of the ESCRT-III dome by the membrane results in the formation of a narrowing membrane neck (Fig. 6 *b*): the larger the membrane affinity to the dome surface, the narrower the neck that will be formed. If the radius of the neck reaches the critical value of about $r_{neck} \approx 2.8$ nm (which corresponds to the water lumen radius close to 1 nm), the neck is predicted to undergo fission (24). Given this, we analyzed computationally the formation and fission of the membrane neck in an analogous manner to the previous study (22), but taking into account that the fission site is connected to the membrane tube with diameter of about $D_{out} \approx 1$ μm (6) rather than to a small spherical membrane bud as in (22). The computed shapes of the membrane neck at sequential stages of the membrane attachment to the ESCRT-III dome are presented in Fig. 6 *b*. Our analysis shows that the values of the membrane affinity to the dome surface, ε, required for neck fission constitute $\varepsilon \approx 0.07$ mN/m, which is smaller by more than an order of magnitude than the estimated value $\varepsilon \approx 3.45$ mN/m inferred from in vitro studies (22). This means that once the membrane is constricted, the affinity of the membrane to the ESCRT-III complex is able to account for ESCRT-III-mediated fission. This analysis completes and confirms the proposed model for ESCRT-assisted cytokinetic abscission.

DISCUSSION

In this study, we suggest and substantiate by experimental and computational data a biophysical mechanism by which ESCRT-III drives abscission of the intercellular bridge in cytokinesis. In the proposed model (Fig. 1), ESCRT machinery assembles on the rims of each side of the midbody dark zone, forming a series of cortical rings beneath the plasma membrane with diameter >1 μm (6). Close to the time of the first abscission event, one of these ESCRT-III initial ring structures begins polymerizing away from the dark zone. The emerging ESCRT-III helical polymer is then acted on by VPS4, which by remodeling the polymer leads to its breakage into two separate structures. The initial structure remains attached to the midbody dark zone, keeping its initial diameter of >1 μm. The second structure, the fission complex, constricts to a preferred diameter of

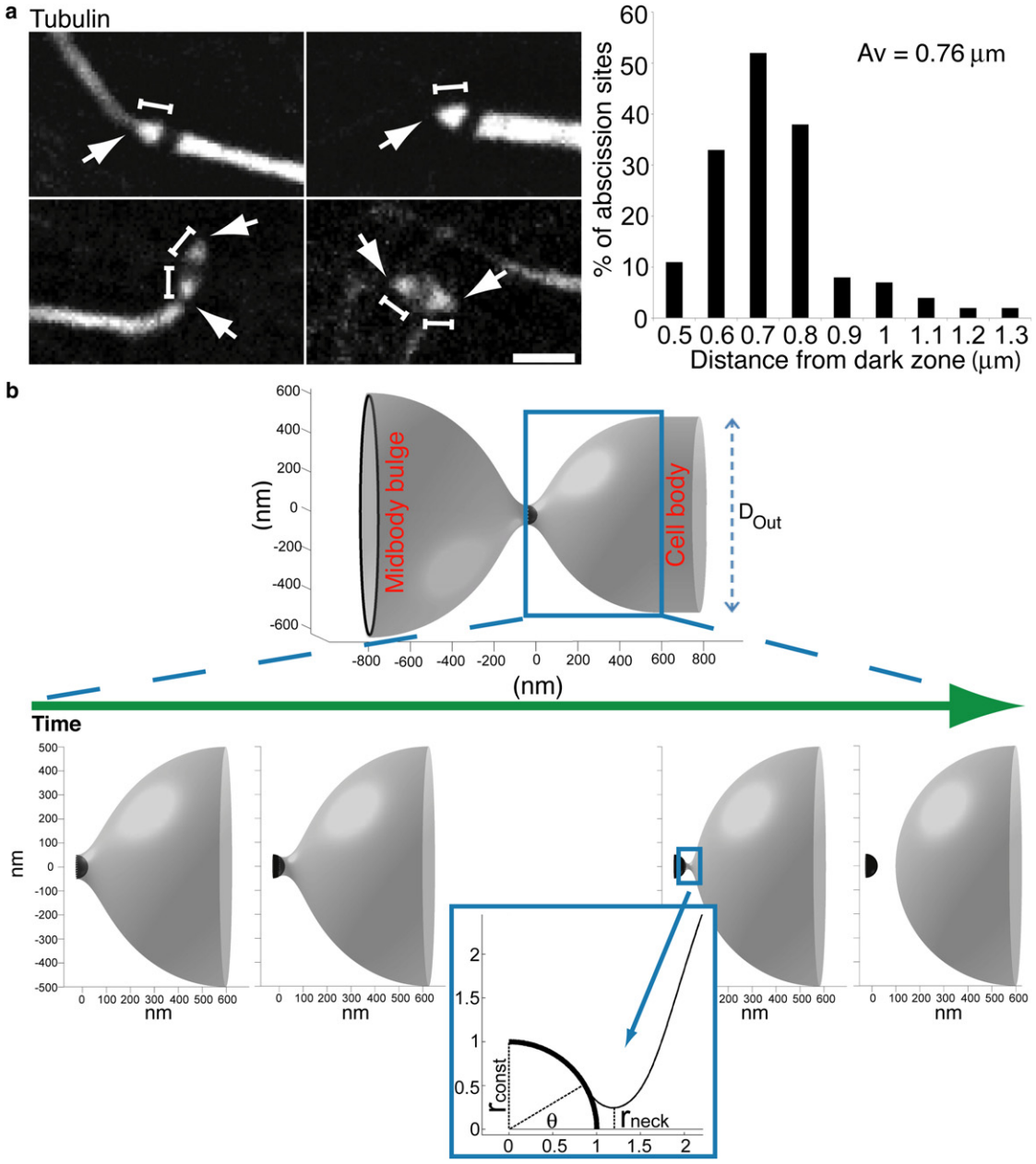

FIGURE 6 Experimental verification of the equilibrium distance and theoretical modeling of ESCRT-III-mediated membrane fission in cytokinesis. (*a*) Testing the equilibrium distance in cells undergoing abscission. The distance between the end of the midbody dark zone and the site of microtubule constriction was measured in synchronized MDCK cells stained with anti-α-tubulin antibodies (*white*). Images on the left are representative examples for the different types of intercellular bridges chosen for this analysis. Arrows represent the sites of constriction/scission and bars represent the distances measured. The histogram to the right shows the distribution of the measured distances. A preferred distance of 0.6–0.8 μm between the edge of the dark zone and the site of microtubule constriction was observed in the majority of intercellular bridges that were examined. The total average for all measurements was 0.76 $\pm$ 0.15 μm. Data were obtained from two independent experiments. $n = 157$. Scale bars $= 2$ μm. (*b*) Computational analysis of ESCRT-III-mediated final fission in cytokinetic abscission. Upper panel shows entire system configuration after constriction of the abscission site to a 0.1 μm diameter for better visualization. The diameter of the cell body is taken $D_{out} = 1$ μm. Framed window represents the membrane neck committed to fission described in details in the image sequence below. Lower panel shows the computed configurations of the membrane neck formed at sequential stages of the membrane attachment to the dome-like end-cap of the ESCRT-III fission complex at the abscission site. The first to third panels (left to right) represent the neck configurations at increasing attachment angles $\theta = 0°$, 30°, 62°, respectively. The fourth panel shows a postfission state where the midbody and cell are separated. Inset: zoom into the constriction site. The dome radius r_{const} is taken to be10 times smaller than the radius r_{out} of the tube connecting the fission site to the body of the daughter cell.

50 nm (characteristic of ESCRT-III filaments in vitro), although remaining persistently bound to the membrane of the intercellular bridge. This constriction results in the membrane deformation and generation of elastic forces within the membrane that drives movement of the fission complex along the intercellular bridge away from the midbody until it reaches an equilibrium position. This process, which culminates in the constriction of the intracellular bridge, is followed by ESCRT-III-mediated fission of the bridge membrane. Driven by membrane attachment to the dome-like end-cap of the fission complex, the fission event leads to complete separation of the two daughter cells. Once this has happened, a second ESCRT-III-mediated cleavage occurs on the other side of the midbody dark zone through the same mechanism as described previously, resulting in release of a midbody remnant.

Localization of different ESCRT-III components to both the midbody center and the abscission site was recently reported (6,7). However, it remained unclear whether the ESCRT-III formed a continuous structure stretching all the way from the rim of the midbody dark zone to the narrow constriction site or, as suggested by our model, resided in two spatially distinct structures. Our detailed experimental analysis of different ESCRT-III components supports the second possibility. Using FLAG-tagged versions of different ESCRT-III components and quantitatively determining their distribution at different time periods during the abscission process, we provide supporting evidence that the ESCRT-III complex eventually resides in two distinct pools having a conserved interdistance, and with the more peripheral pool residing at the abscission site. EM tomography data, showing ESCRT-III dependent helical spirals restricted to constriction sites (7), further favor the existence of two distinct ESCRT-III pools.

An attractive feature of our model for ESCRT-III driven cytokinetic abscission is that it accounts for the perplexing observation of two pools of ESCRT-III in the midbody region. The two pools originate from breakage of one initial pool polymerizing at the edge of the midbody dark zone. Notably, this breakage allows one of the emerging ESCRT-III complexes, the fission complex, to slide away from the initial complex and undergo constriction. As mentioned previously, our experimental data support the emergence of the ESCRT-III fission complex from the ESCRT-III initial complex but do not provide an ultimate proof for it. Therefore, further experiments using higher spatiotemporal resolution are still needed to substantiate this aspect of the model.

The direct measurements of the distance between the two ESCRT-III pools during cytokinetic abscission that we have performed suggest that constriction of the cytokinetic bridge proceeds in two steps. According to our measurements, the second ESCRT-III structure already reaches its equilibrium position (located at a 0.7 μm away from the edge of the midbody dark zone) in intercellular bridges with a diameter of 0.4 μm (Fig. 3). From this point on constriction of the bridge continues with no further movement of the second ESCRT-III structure. This means that an additional step is required for the final constriction of the bridge from 0.4 μm down to 50 nm. One attractive possibility is that microtubule removal, which was previously shown to be necessary for completion of cytokinetic abscission, is required in order to constrict the bridge to a diameter smaller than 0.4 μm. Indeed, the microtubule severing enzyme spastin was shown to bind to the ESCRT-III component CHMP1B and to colocalize with the second ESCRT-III structure (7,25,26). Of importance, deletion of spastin delayed abscission but did not prevent the formation of cortical filaments at the constriction zones (7), supporting a role for spastin downstream to the formation of the ESCRT-III fission complex.

It is still not clear what mediates breakage of the initial ESCRT-III polymer. A likely factor, however, is the AAA-ATPase VPS4, because it remodels ESCRT-III filaments through disassembly (18,27). ESCRT-III and VPS4 are the only ESCRT components conserved from archea to humans and required for membrane constriction during cytokinesis (17,28,29). VPS4 activity, therefore, appears to be important for ESCRT-III-mediated membrane remodeling. VPS4 activity could potentially initiate remodeling of ESCRT-III polymer extending off the large diameter midbody pool. Consistent with this role, ESCRT-III polymer breakage during cytokinesis was inhibited by ATP depletion, a condition that inhibits VPS4 activity. Under these circumstances, a continuous ESCRT-III polymer was seen extending a significant distance from the midbody center.

What regulates the nucleation and polymerization of ESCRT-III that leads to the formation of the ESCRT-III fission complex is yet to be determined. Membrane trafficking and endosomal fusion have been previously suggested to mediate the narrowing of the cytokinetic bridge during abscission (3,4,30) and the ESCRT machinery has been shown in vitro to have a strong preference to acidic membranes (5,8,13). A plausible scenario, therefore, is that the membrane trafficking events that precede abscission facilitate a change in the lipid composition of the intercellular bridge membrane, which is needed for the activities of the ESCRT-III fission complex.

Whether ESCRT-III polymerization coupled with breakage and sliding of a constricting membrane-bound ESCRT-III complex to a location corresponding to minimal elastic energy of the membrane is a conserved property of other ESCRT-mediated processes (i.e., human immunodeficiency virus budding and intraluminal vesicle budding into multivesicular bodies) remains to be explored. That said, recent work suggests that the filamentous GTP-dependent FtsZ complex in bacteria mediates membrane constriction events during bacterial cytokinesis in a similar manner to the mechanism proposed here for ESCRT-III-mediated cytokinetic abscission (31). The FtsZ complex was shown to assemble into large diameter cortical rings that slide along tubular liposomes and constrict the membrane. Remodeling

of the FtsZ polymer was crucial for its activity in membrane constriction because when GTP hydrolysis was inhibited, sliding of the FtsZ rings stopped and no significant membrane constriction occurred. A common feature of membrane-bound helical filamentous systems undergoing membrane constriction, therefore, may be polymerization and filament remodeling/breakage, as described and modeled here.

We thank Dr. Ramanujan Hegde (National Institutes of Health) for kindly providing the rabbit polyclonal Flag antibodies. We thank Alan Hoofring from the National Institutes of Health medical art design section for help with the illustration. We also thank members of the Hurly lab and members of the J.L.-S. lab for fruitful discussion. N.E. conducted all the experiments. N.E. and J.L.-S. designed the experiments. G.F. and M.M.K. performed all the computational modeling. N.E., M.M.K., and J.L.-S. wrote the manuscript. The authors declare no conflict of interest.

J.L.-S. was supported by the Intramural program of the National Institutes of Health, the Intramural Program of Eunice Shriver National Institute of Child Health and Development, and Intramural AIDS Targeted Antiviral Program. M.M.K. was supported by the Israel Science Foundation and the Marie Curie Network "Virus Entry".

REFERENCES

1. Eggert, U. S., T. J. Mitchison, and C. M. Field. 2006. Animal cytokinesis: from parts list to mechanisms. *Annu. Rev. Biochem.* 75:543–566.
2. Steigemann, P., and D. W. Gerlich. 2009. Cytokinetic abscission: cellular dynamics at the midbody. *Trends Cell Biol.* 19:606–616.
3. Schiel, J. A., and R. Prekeris. 2010. Making the final cut - mechanisms mediating the abscission step of cytokinesis. *ScientificWorldJournal.* 10:1424–1434.
4. Neto, H., L. L. Collins, and G. W. Gould. 2011. Vesicle trafficking and membrane remodelling in cytokinesis. *Biochem. J.* 437:13–24.
5. Caballe, A., and J. Martin-Serrano. 2011. ESCRT machinery and cytokinesis: the road to daughter cell separation. *Traffic.* 12:1318–1326.
6. Elia, N., R. Sougrat, …, J. Lippincott-Schwartz. 2011. Dynamics of endosomal sorting complex required for transport (ESCRT) machinery during cytokinesis and its role in abscission. *Proc. Natl. Acad. Sci. USA.* 108:4846–4851.
7. Guizetti, J., L. Schermelleh, …, D. W. Gerlich. 2011. Cortical constriction during abscission involves helices of ESCRT-III-dependent filaments. *Science.* 331:1616–1620.
8. Lata, S., G. Schoehn, …, W. Weissenhorn. 2008. Helical structures of ESCRT-III are disassembled by VPS4. *Science.* 321:1354–1357.
9. Carlton, J. G., and J. Martin-Serrano. 2007. Parallels between cytokinesis and retroviral budding: a role for the ESCRT machinery. *Science.* 316:1908–1912.
10. Morita, E., V. Sandrin, …, W. I. Sundquist. 2007. Human ESCRT and ALIX proteins interact with proteins of the midbody and function in cytokinesis. *EMBO J.* 26:4215–4227.
11. Morita, E., L. A. Colf, …, W. I. Sundquist. 2010. Human ESCRT-III and VPS4 proteins are required for centrosome and spindle maintenance. *Proc. Natl. Acad. Sci. USA.* 107:12889–12894.
12. McDonald, B., and J. Martin-Serrano. 2009. No strings attached: the ESCRT machinery in viral budding and cytokinesis. *J. Cell Sci.* 122:2167–2177.
13. Wollert, T., D. Yang, …, J. H. Hurley. 2009. The ESCRT machinery at a glance. *J. Cell Sci.* 122:2163–2166.
14. Wollert, T., and J. H. Hurley. 2010. Molecular mechanism of multivesicular body biogenesis by ESCRT complexes. *Nature.* 464:864–869.
15. Wollert, T., C. Wunder, …, J. H. Hurley. 2009. Membrane scission by the ESCRT-III complex. *Nature.* 458:172–177.
16. Saksena, S., J. Wahlman, …, S. D. Emr. 2009. Functional reconstitution of ESCRT-III assembly and disassembly. *Cell.* 136:97–109.
17. Davies, B. A., M. Babst, and D. J. Katzmann. 2011. Regulation of Vps4 during MVB sorting and cytokinesis. *Traffic.* 12:1298–1305.
18. Davies, B. A., I. F. Azmi, …, D. J. Katzmann. 2010. Coordination of substrate binding and ATP hydrolysis in Vps4-mediated ESCRT-III disassembly. *Mol. Biol. Cell.* 21:3396–3408.
19. Hurley, J. H., and P. I. Hanson. 2010. Membrane budding and scission by the ESCRT machinery: it's all in the neck. *Nat. Rev. Mol. Cell Biol.* 11:556–566.
20. Hanson, P. I., R. Roth, …, J. E. Heuser. 2008. Plasma membrane deformation by circular arrays of ESCRT-III protein filaments. *J. Cell Biol.* 180:389–402.
21. Peel, S., P. Macheboeuf, …, W. Weissenhorn. 2011. Divergent pathways lead to ESCRT-III-catalyzed membrane fission. *Trends Biochem. Sci.* 36:199–210.
22. Fabrikant, G., S. Lata, …, M. M. Kozlov. 2009. Computational model of membrane fission catalyzed by ESCRT-III. *PLOS Comput. Biol.* 5:e1000575.
23. Helfrich, W. 1973. Elastic properties of lipid bilayers: theory and possible experiments. *Z. Naturforsch. C.* 28:693–703.
24. Kozlovsky, Y., and M. M. Kozlov. 2003. Membrane fission: model for intermediate structures. *Biophys. J.* 85:85–96.
25. Connell, J. W., C. Lindon, …, E. Reid. 2009. Spastin couples microtubule severing to membrane traffic in completion of cytokinesis and secretion. *Traffic.* 10:42–56.
26. Yang, D., N. Rismanchi, …, J. H. Hurley. 2008. Structural basis for midbody targeting of spastin by the ESCRT-III protein CHMP1B. *Nat. Struct. Mol. Biol.* 15:1278–1286.
27. Babst, M., B. Wendland, …, S. D. Emr. 1998. The Vps4p AAA ATPase regulates membrane association of a Vps protein complex required for normal endosome function. *EMBO J.* 17:2982–2993.
28. Samson, R. Y., T. Obita, …, S. D. Bell. 2008. A role for the ESCRT system in cell division in archaea. *Science.* 322:1710–1713.
29. Lindås, A. C., E. A. Karlsson, …, R. Bernander. 2008. A unique cell division machinery in the Archaea. *Proc. Natl. Acad. Sci. USA.* 105:18942–18946.
30. Schiel, J. A., K. Park, …, R. Prekeris. 2011. Endocytic membrane fusion and buckling-induced microtubule severing mediate cell abscission. *J. Cell Sci.* 124:1411–1424.
31. Osawa, M., and H. P. Erickson. 2011. Inside-out Z rings—constriction with and without GTP hydrolysis. *Mol. Microbiol.* 81:571–579.